

Extraction of Proton Trace Anomaly Energy from Near-Threshold ϕ and J/ψ photo-productions

Wei Kou,^{1,2} Rong Wang,^{1,2,*} and Xurong Chen^{1,2,3,†}

¹*Institute of Modern Physics, Chinese Academy of Sciences, Lanzhou 730000, China*

²*University of Chinese Academy of Sciences, Beijing 100049, China*

³*Guangdong Provincial Key Laboratory of Nuclear Science, Institute of Quantum Matter, South China Normal University, Guangzhou 510006, China*

The trace anomalous energy contribution to the proton mass is a very important topic in non-perturbative QCD and hadron physics. In experiments, it is under the hot discussions on how to measure the trace anomalous energy. The QCD interpretation of proton trace anomaly is still not clear. To connect the theory with the experiment, we extract the trace anomaly by analyzing the near-threshold photo-production data of ϕ and J/ψ vector mesons. Based on the vector-meson-dominance model and QCD Van der Waals representation, we find that the percentage of trace anomaly in the proton mass ranges from 16% to 24%, which is of similar order of magnitude as the 23% given by Lattice QCD. We also provide the approximate magnitudes of the systematic uncertainties of the extracted results from the model assumptions as well as the data fitting procedures. We give relative statistical uncertainties of 17.2%, 17.7%, 3.6%, and 8.2%, total relative systematic uncertainties of 21.4%, 54.2%, 37.2%, and 25.7%, for the analyses of the GlueX, LEPS, CLAS, and SAPHIR data, respectively. We argue that the near-threshold Υ photo-production experiments are more beneficial for the measurement of trace anomaly in proton mass in the future.

I. INTRODUCTION

The majority of the visible mass of the universe resides in the two types of nucleons – protons and neutrons. Nucleons are made of massless gluons and almost massless quarks. The generation of nucleon mass is one of the puzzles in modern particle physics. The origin of the masses of fundamental particles (leptons, quarks, and massive gauge bosons) are delicately explained by the famous Higgs mechanism [1–3]. The proton mass comes mainly from the complicated workings of non-perturbative Quantum Chromodynamics (QCD) [4–6]. QCD theory originates from Yang-Mills theory [7] in the 1950s, which belongs to a non-abelian gauge theory. To calculate the proton mass in the first principle view, one encounters two main challenges: the color confinement for the constituents (quarks and gluons) [8] and the divergent strong coupling constant at low energy scale.

The proton is a composite particle made of quarks and gluons, hence its mass is usually argued to be from some different sources. The concept of trace anomaly was first introduced from Refs. [9, 10]. In Refs. [11, 12], Ji first define the proton mass decomposition with QCD Hamiltonian operators. Four gauge-invariant Hamiltonian operators are introduced as,

$$H_{\text{QCD}} = H_q + H_g + H_m + H_a, \quad (1)$$

where

$$\begin{aligned} H_q &= \int d^3\vec{x} [\psi^\dagger(-i\mathbf{D}\cdot\alpha)\psi], \\ H_g &= \int d^3\vec{x} \frac{1}{2} (\mathbf{E}^2 + \mathbf{B}^2), \\ H_m &= \int d^3\vec{x} \left(1 + \frac{1}{4}\gamma_m\right) \bar{\psi}m\psi, \\ H_a &= \int d^3\vec{x} \frac{1}{4}\beta(g) (\mathbf{E}^2 - \mathbf{B}^2). \end{aligned} \quad (2)$$

In Ref. [12], the author assumed that the hadron mass is calculated as the expectation value of the Hamiltonian at the hadron rest frame:

$$M_N = \frac{\langle P | H_{\text{QCD}} | P \rangle}{\langle P | P \rangle} \Big|_{\text{rest frame}}, \quad (3)$$

which is decomposed into four terms characterized by the QCD trace anomaly parameter $b(\mu^2)$ and the momentum fraction $a(\mu^2)$ carried by all quarks [12]. The four terms of the proton mass partitions are written as [12],

$$\begin{aligned} M_q &= \frac{3}{4} \left(a - \frac{b}{1 + \gamma_m} \right) M_N, \quad M_g = \frac{3}{4} (1 - a) M_N, \\ M_m &= \frac{4 + \gamma_m}{4(1 + \gamma_m)} b M_N, \quad M_a = \frac{1}{4} (1 - b) M_N, \end{aligned} \quad (4)$$

where the anomalous dimension of quark mass γ_m [13] describes the renormalization information. The momentum fraction $a(\mu^2)$ of the quarks is easily computed with all the quark distributions determined in experiments as,

$$a(\mu^2) = \sum_f \int_0^1 x [q_f(x, \mu^2) + \bar{q}_f(x, \mu^2)] dx. \quad (5)$$

* rwang@impcas.ac.cn

† xchen@impcas.ac.cn

The proton mass decomposition is from the analysis of the energy-momentum tensor (EMT) in QCD theory [12]. The first three terms in Eq. (4) can be easily understood with the classical field theory. However the last term is an extension of the classical description in the quantum field theory – the quantum anomaly. In the recent papers [14, 15], the authors provide further discussion on the source of quantum anomalous energy (QAE) to the proton mass and argue that it arises from the scale symmetry breaking due to the ultraviolet (UV) divergences in the quantum field theories. The trace anomaly part to the proton mass resembles the dynamical Higgs mechanism to the mass of the fundamental fermions. The author mentions that the quantum anomalous contribution is scale-independent in the chiral limit [14]. However the quark mass is not exactly zero. Therefore, the quantum anomalous energy should be scale-dependent due to the contribution of the quark mass [16, 17].

Although the proton mass is mainly generated by the dynamical chiral symmetry breaking, a small portion does arise from the masses of the quarks. The quark mass contribution is usually characterized by a matrix element parameter b [12], which is used to represent the Hamiltonian of quark mass term in Eqs. (2) and (4). The parameter b is related to the quark masses themselves and the quark scalar charges of the proton [10, 12],

$$\begin{aligned} bM_N &= \langle N | m_u \bar{u}u + m_d \bar{d}d | N \rangle + \langle N | m_s \bar{s}s | N \rangle \\ &= m_l \langle N | \bar{u}u + \bar{d}d | N \rangle + m_s \langle N | \bar{s}s | N \rangle \\ &= \sigma_{\pi N} + \sigma_{sN}. \end{aligned} \quad (6)$$

The scalar nucleon matrix element of up and down quarks $\sigma_{\pi N}$ is about 45 MeV, determined by the low energy $\pi - N$ scattering amplitude [18–20]. In Ref. [21], the authors present a new result using new experimental data and chiral effective field theory $\sigma_{\pi N} = 59(7)$ MeV. Phenomenological estimation using $\pi - N$ scattering data was performed in the Ref. [22]. Too little is known about the σ_{sN} , which describes the strange scalar charge $m_s \langle N | \bar{s}s | N \rangle$ in the nucleon [10, 11]. It is believed to be large because the strange quark is heavier. However, in theory, the QCDSF Collaboration finds $\sigma_{sN} = 11 \pm 13$ MeV [23] and the χ QCD Collaboration finds $\sigma_{sN} = 40 \pm 12$ MeV [24]. The strange part of nucleon matrix element σ_{sN} is also suggested to be small around 16 MeV from an effective field theory [25]. The nucleon scalar charge is an important parameter for calculating the scattering between nucleon and the dark matter particles [26–31]. Hence studying the QCD trace anomaly parameter b might be helpful in investigating the method of detecting the weakly-interacting dark matter particles.

At present, the direct experimental measurement of quantum effects inside protons is impossible to be realized. But the low-energy scattering between heavy quarkonium and nucleon can be used to probe the trace anomaly of the nucleon, since the two-gluon exchange is dominant for the process [16, 17, 32, 33]. It is not difficult to compute the scattering amplitude using the local

operator product expansion (OPE) with the gluon operator [34]. Recently, in Refs. [35, 36] the authors had tried to extract the trace anomaly from the J/ψ photo-production data near threshold, based on a holographic QCD framework. Based on the Lattice QCD, the result of proton anomaly is discussed in Ref. [37]. For more information on the importance of the proton trace anomaly, one can refer to the EICUG Yellow Report [38]. In this work, we begin with the vector-meson-dominance model (VMD) suggested by Refs. [10, 39]. Following the recent analysis based on this method [40], we try to extract the trace anomalous energy of the proton firstly from the diffractive production data of both ϕ and J/ψ vector mesons near the thresholds [41, 42]. The paper is organized as follows. We describe the forward meson-nucleon scattering amplitude in the VMD model in Sec. II, relating the parameter b to the photo-production data. We subsequently show our extraction of the trace anomaly part by fitting the experimental data in Sec. III. We generally discuss and analyze the uncertainties introduced by the model and data fitting in Sec. IV. Finally we give the conclusions and discussions in Sec. V.

II. METHOD

With the VMD model [43], the forward cross section of the vector meson X (ϕ , J/ψ , Υ , etc.) photo-production on the nucleon target is formulated as [39],

$$\begin{aligned} & \left. \frac{d\sigma_{\gamma N \rightarrow XN}}{dt} \right|_{t=0} \\ &= \frac{3\Gamma(X \rightarrow e^+e^-)}{\alpha m_X} \left(\frac{k_{XN}}{k_{\gamma N}} \right)^2 \left. \frac{d\sigma_{XN \rightarrow XN}}{dt} \right|_{t=0}, \end{aligned} \quad (7)$$

where $\alpha = 1/137$ denotes the fine structure constant, $k_{ab}^2 = [s - (m_a + m_b)^2][s - (m_a - m_b)^2]/4s$ describes the center-of-mass momentum square of the corresponding two-body system, and Γ is the partial decay width of the X meson decaying into a e^+e^- pair. The $\left. \frac{d\sigma_{XN \rightarrow XN}}{dt} \right|_{t=0}$ term of elastic scattering in the forward limit is given by,

$$\left. \frac{d\sigma_{XN \rightarrow XN}}{dt} \right|_{t=0} = \frac{1}{64\pi} \frac{1}{m_X^2 (\lambda^2 - m_N^2)} |F_{XN}|^2, \quad (8)$$

where $\lambda = (p_N p_X / m_X)$ is the nucleon energy at the quarkonium rest frame [39]. F_{XN} denotes the invariant amplitude of $X - N$ elastic scattering. Using these definitions, the amplitude takes the form [10, 39],

$$\begin{aligned} F_{XN} &\simeq r_0^3 d_2 \frac{8\pi^2 M_N m_X}{27} \left(M_N - \left\langle N \left| \sum_{i=u,d,s} m_i \bar{q}_i q_i \right| N \right\rangle \right) \\ &= r_0^3 d_2 \frac{8\pi^2}{27} (1-b) M_N^2 m_X, \end{aligned} \quad (9)$$

which is dominated by the QCD trace anomaly part. For low-energy scattering and in the chiral limit, the mass of a hadron state comes purely from the quantum fluctuations of the gluons. Away from the chiral limit, the factor $(1 - b)$ is used to characterize the QCD trace anomaly contribution to the proton mass. In Eq. (9), the “Bohr” radius r_0 of the meson X is given by [10],

$$r_0 = \left(\frac{4}{3\alpha_s} \right) \frac{1}{m_q}, \quad (10)$$

where m_q represents the mass of quark (strange quark s for the ϕ meson and charm quark c for the J/ψ meson). In this work, we choose the constituent quark mass (low-energy scale) for the extraction, e.g. $m_c = 1.67$ GeV and $m_s = 0.486$ GeV [44]. We discuss the effect of quark mass selection on the results in the final section. In Eq. (9), the Wilson coefficient d_2 is found in Refs. [10, 45, 46] as,

$$d_n^{(1S)} = \left(\frac{32}{N_c} \right)^2 \sqrt{\pi} \frac{\Gamma(n + \frac{5}{2})}{\Gamma(n + 5)}, \quad (11)$$

where N_c is the number of colors. The strong coupling constant α_s depends on the renormalization scale μ^2 , and the scale is chosen to be the “Rydberg” energy square ϵ_0^2 for the bound state of the quarkonium X [10, 46].

The running strong coupling constant α_s is an important parameter in QCD evolution equations. In this work, we use a renormalization-group-invariant process-independent effective strong coupling constrained by the calculation of LQCD [47]. The effective strong coupling shows a saturated plateau approaching the infrared region, which agrees well with the Bjorken sum rule with meson PDFs at low $\mu^2 (< 1 \text{ GeV}^2)$ [47]. The saturated effective strong coupling is given by [47, 48],

$$\alpha_s(\mu^2) = \frac{4\pi}{\beta_0 \ln \left[(m_\alpha^2 + \mu^2) / \Lambda_{\text{QCD}}^2 \right]}, \quad (12)$$

where $\beta_0 = (33 - 2n_f)/3$ refers to the one-loop β function coefficient, n_f is the number of flavors, $m_\alpha = 0.43$ GeV is the effective gluon mass owing to the dynamical breaking of scale invariance [47]. For the QCD cutoff, we chose $\Lambda_{\text{QCD}} = 0.34$ GeV [49]. Based on this analysis, we use the saturated form of strong coupling in order to take into account of the non-perturbative effect.

Applying the theoretical and phenomenological framework discussed above, we extract the QCD trace anomaly M_a from the extrapolated value of the differential photo-production cross section at Mandelstam variable $-t = 0 \text{ GeV}^2$. We take the differential cross section data from the diffractive ϕ photo-production near the threshold published by the LEPS, SAPHIR and CLAS Collaborations [41, 50–52] and the diffractive J/ψ photo-production data near the threshold by GlueX Collaboration at Jefferson Laboratory (JLab) [42]. The experimental data are fitted with an exponential function

$$\frac{d\sigma}{dt} = \frac{d\sigma}{dt} \Big|_{t=0} \times e^{-kt}, \quad (13)$$

where $d\sigma/dt|_{t=0}$ represents the forward differential cross-section and k denotes the slope parameter. Eq. (13) describes the t -dependence of the cross section. The details of our studies and the results are shown in the next section, focusing on the formulae mentioned in this section.

III. EXTRACTION OF TRACE ANOMALY

Based on Eq. (13), the forward differential cross-sections are obtained by fitting the experimental data of ϕ and J/ψ photo-productions near the thresholds from Refs. [41, 42, 50, 51]. According to Eqs. (7-12), the trace anomaly parts of proton mass are extracted by simple algebraic operations. FIG. 1 shows the GlueX collaboration’s near-threshold differential cross section data for J/ψ photo-production on the proton. It is suggested that the $-t$ -dependence of the differential cross section is well described with the exponential form [42].

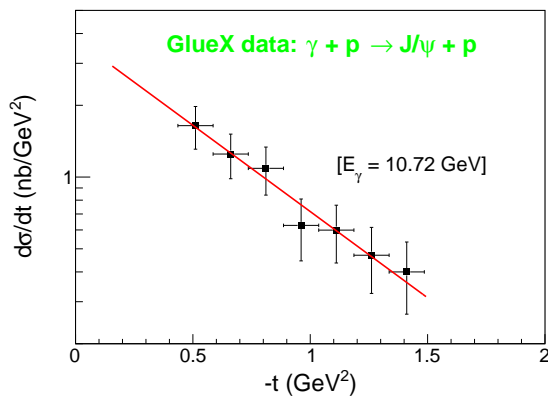


FIG. 1. The differential cross section of J/ψ photo-production near threshold of $E_\gamma = 10.72$ GeV by GlueX Collaboration [42]. The red line shows our fitting result with an exponential form. $\chi^2/d.o.f. = 0.14$. Only statistical uncertainties are shown. The obtained parameters are listed in TABLE I.

TABLE I lists the key parameters and the experimental settings for the extraction of the QCD trace anomaly. In this work we assume that the energy scale of the strong interaction (μ) is equal to the “Rydberg” energy ϵ_0 of the quark-antiquark pair [39, 46], for the production near the threshold. For J/ψ production, the binding energy $\epsilon_0^2 = \mu^2 = 0.41 \text{ GeV}^2$ is taken in Ref. [10]. Thinking about pulling apart a $c\bar{c}$ pair to generate a $D\bar{D}$ pair, a naive estimate of the “Rydberg” energy ϵ_0 is $m_D + m_{\bar{D}} - m_{J/\psi}$ [10, 40]. Similarly, we choose $\epsilon_0^2 = 0.14 \text{ GeV}^2$ as the energy scale corresponding to the ϕ photo-production.

The ϕ production data from CLAS, SAPHIR and LEPS collaborations are presented in FIGS. 2 and 4. We still use the exponential function fittings to get the forward differential cross sections, respectively. In the following paragraphs we present some of the details.

TABLE I. Forward cross section $\frac{d\sigma}{dt}|_{-t=0}$ and trace anomaly M_a/M_N extracted by fitting the experimental data from GlueX collaboration (corresponding to Fig. 1). Only statistical uncertainties are considered. The systematic uncertainty analysis is described in Sec. IV.

E_γ (GeV)	$\frac{d\sigma}{dt} _{-t=0}$ (nb/GeV ²)	$\chi^2/d.o.f.$	M_a/M_N (%)
10.72	3.79 ± 1.32	0.14	19.2 ± 3.3

FIG. 2 shows the LEPS collaboration's near-threshold differential cross section data for ϕ photo-production on the proton target.

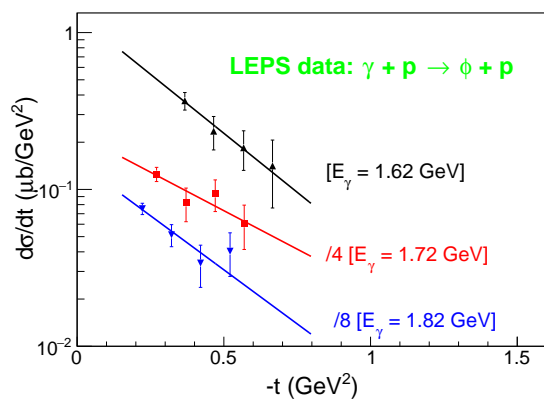


FIG. 2. The differential cross sections of coherent ϕ photo-production on proton near threshold ($\gamma p \rightarrow \phi p$) from LEPS [41]. Only the statistical errors are presented. The cross-section data at $E_\gamma = 1.72$ GeV and $E_\gamma = 1.82$ GeV are divided by 4 and 8 respectively, as indicated in the figure. The solid lines show the fits of exponential form.

The results for some important physical quantities are listed in TABLE II.

TABLE II. Forward cross section $\frac{d\sigma}{dt}|_{-t=0}$ and trace anomaly M_a/M_N extracted by fitting the experimental data from LEPS collaboration (corresponding to Fig. 2). Only statistical uncertainties are considered. The systematic uncertainty analysis is described in Sec. IV.

E_γ (GeV)	$\frac{d\sigma}{dt} _{-t=0}$ ($\mu\text{b}/\text{GeV}^2$)	$\chi^2/d.o.f.$	M_a/M_N (%)
1.62	1.29 ± 0.68	0.10	18.9 ± 4.5
1.72	0.91 ± 0.28	0.60	16.5 ± 2.5
1.82	1.20 ± 0.33	0.66	20.0 ± 2.8

We present the trace anomaly extracted from cross-section data at three energy points near the threshold

measured by the LEPS collaboration [41]. Due to the low statistics, the uncertainty is relatively large. We also analyze the measurements from the SAPHIR collaboration [50] several decades ago for the comparisons. The differential cross section data of SAPHIR are shown in FIG. 3. From the fittings of the exponential form of Eq. (13), the SAPHIR data give the proton trace anomaly parts to be $18.3 \pm 1.8\%$ and $16.9 \pm 1.1\%$ at $E_\gamma = 1.7$ GeV and $E_\gamma = 1.95$ GeV, respectively (summarized in TABLE III).

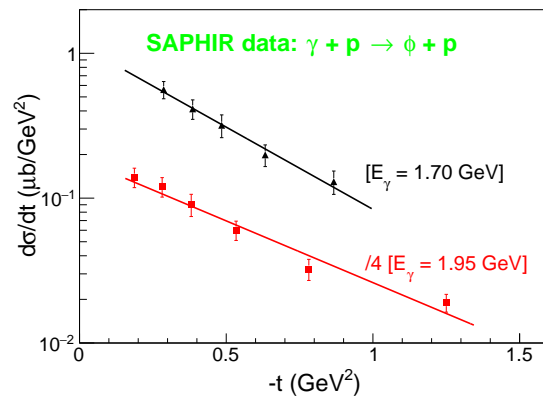


FIG. 3. The differential cross sections of coherent ϕ photo-production on proton near threshold ($\gamma p \rightarrow \phi p$) from SAPHIR [50]. Only the statistical errors are presented. The cross-section data at $E_\gamma = 1.95$ GeV is divided by 4, as indicated in the figure. The solid lines show the fits of exponential form.

TABLE III. Forward cross section $\frac{d\sigma}{dt}|_{-t=0}$ and trace anomaly M_a/M_N extracted by fitting the experimental data from SAPHIR collaboration (corresponding to Fig. 3). Only statistical uncertainties are considered. The systematic uncertainty analysis is described in Sec. IV.

E_γ (GeV)	$\frac{d\sigma}{dt} _{-t=0}$ ($\mu\text{b}/\text{GeV}^2$)	$\chi^2/d.o.f.$	M_a/M_N (%)
1.70	1.14 ± 0.23	0.21	18.3 ± 1.8
1.95	0.74 ± 0.10	1.11	16.9 ± 1.1

Due to the high luminosity of the accelerator and the large acceptance of the CLAS spectrometer, the CLAS data is of high precision over a wide $-t$ range [51, 52]. In the following, we perform a similar analysis on the CLAS data on the proton. Fig. 4 shows the CLAS collaboration's near-threshold differential cross section data for ϕ photo-production on the hydrogen target. The fits to the data based on Eq. (13) are shown in the figure. The differential cross section data are described reasonably well by the exponential function. However in the large $-t$ region, we see the cross section rising with $-t$. This behavior in the large $-t$ region may be due to the direct

ϕ -radiation contributions from u -channel and s -channel with ϕNN coupling or ϕNN^* coupling [53–60].

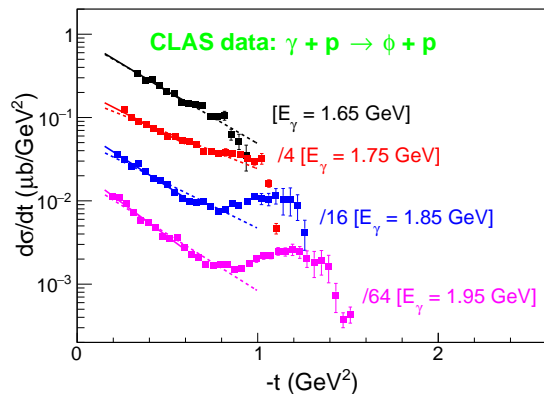


FIG. 4. The differential cross sections of near-threshold ϕ photo-production on a hydrogen target ($\gamma p \rightarrow \phi p$) from CLAS [51, 52]. Only the statistical errors are presented. Some of the cross sections are scaled by factors indicated in the figure. The dashed lines show the fits in the $-t$ range from 0.15 GeV^2 to 1 GeV^2 . The solid lines show the fits in the $-t$ range from 0.15 to 0.6 GeV^2 .

TABLE IV. Forward cross section $\frac{d\sigma}{dt}|_{-t=0}$ and trace anomaly M_a/M_N extracted by fitting the experimental data from CLAS collaboration (corresponding to Fig. 4). Only statistical uncertainties are considered. The systematic uncertainty analysis is described in Sec. IV.

E_γ (GeV)	$\frac{d\sigma}{dt} _{-t=0}$ ($\mu\text{b}/\text{GeV}^2$)	$\chi^2/d.o.f.$	M_a/M_N (%)
1.65	0.93 ± 0.10	1.28	16.0 ± 0.9
1.75	0.89 ± 0.06	1.70	16.6 ± 0.6
1.85	1.18 ± 0.06	2.41	20.2 ± 0.5
1.95	1.52 ± 0.07	3.04	24.2 ± 0.6

The fitting qualities and extraction of trace anomaly are summarized in TABLE IV. To avoid the u -channel or s -channel contamination, we narrow the fit range to the small $-t$ region. We carefully studied the fits restricted to different $-t$ ranges, as the CLAS data covers a wide $-t$ range and of high precision. To understand the effect of large $-t$ data on the extraction of forward differential cross section and trace anomaly, we perform a series of fits excluding the large $-t$ data requiring $-t < 0.6 \text{ GeV}^2$, $-t < 0.7 \text{ GeV}^2$, $-t < 0.8 \text{ GeV}^2$, $-t < 0.9 \text{ GeV}^2$ and $-t < 1.0 \text{ GeV}^2$ respectively. The proton trace anomaly obtained from these fits are shown in FIG. 5. We find that below 1 GeV^2 , the extracted trace anomaly does not strongly depend on the choice of large $-t$ cuts. This is probably because the u -channel or s -channel contribution

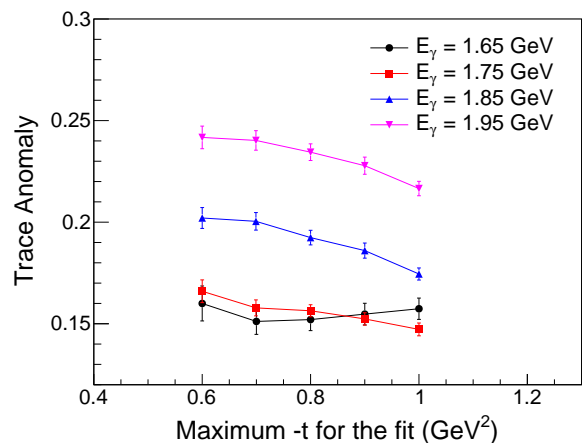


FIG. 5. The proton trace anomaly as a function of the maximum $-t$ in the fitting range, extracted from CLAS data.

only dominates in the large- $-t$ region where the error bars are comparatively large [54–60]. Therefore, the large $-t$ data have little effect on the fits. The uncertainty arising from changing the fit range of $-t$ is consistent with the statistical uncertainty in the data.

IV. UNCERTAINTY ANALYSIS

Now let us try to systematically estimate the uncertainty of the analysis in the previous section. From the method we used to extract the trace anomaly, the forward scattering cross sections are fitted from the data and the model calculating the $X - N$ elastic scattering amplitude (9), which result in the statistical and systematic uncertainties. We start with the model and consider the uncertainty that may arise from the selection of the model’s arguments. It can be seen in Eq. (9) that the $X - N$ elastic scattering amplitude depends on the previously mentioned “Bohr” radius r_0 . In Eq. (10), the expression tells us that the “Bohr” radius of vector meson depends on the quark mass m_q and the strong coupling constant α_s . First, we take the results in Tables I and II as the benchmarks ($m_s = 0.486 \text{ GeV}$ and $m_c = 1.67 \text{ GeV}$). Then we consider the quark masses with 5% fluctuations, i.e. $m_{q\pm} = m_q(1 \pm 5\%)$. The trace anomaly $\frac{1}{4}(1 - b)$ obtained for different quark masses are shown in the following tables.

TABLE V. Trace anomaly contributions (in percentage) to the proton mass with different values of strange quark mass based on LEPS data [41].

E_γ (GeV)	m_{s-}	m_s	m_{s+}	Mean Deviation
1.62	15.9 ± 4.2	18.5 ± 4.9	21.4 ± 5.6	2.75
1.72	14.1 ± 2.2	16.5 ± 2.5	19.1 ± 2.9	2.5
1.82	17.2 ± 2.4	20.0 ± 2.8	23.2 ± 3.2	3.0

TABLE VI. Trace anomaly contributions (in percentage) to the proton mass with different values of charm quark mass based on GlueX data [42].

E_γ (GeV)	m_{c-}	m_c	m_{c+}	Mean Deviation
10.72	16.5 ± 2.9	19.2 ± 3.3	22.3 ± 3.9	2.9

Tables. V and VI show the mean deviation of the trace anomaly for different quark masses for each E_γ set. We easily get a relative deviation in the order of 15%, i.e. 5% of the quark mass fluctuations cause 15% deviation of the extracted trace anomaly. For the impact of the uncertainty of strong coupling α_s , we perform the same analysis as that with the quark mass. We take the uncertainty of the coupling constant in Ref. [19] and fix the fluctuation of α_s at the level of 5%. Then we find that the trace anomaly also has 15% deviation with different strong couplings.

The extracted proton trace anomaly from the experiments also relies on the data fitting settings. We consider the statistical uncertainty in the experimental data in the previous discussions. As a supplement, we try to discuss some additional uncertainties that exist in terms of experiments. We consider the standard deviations associated with different fitting ranges for the Mandelstam's variable $|-t|$ for different energy cases of the CLAS data [51, 52]. A series of fits excluding the large $-t$ data requiring $-t < 0.6 \text{ GeV}^2$, $-t < 0.7 \text{ GeV}^2$, $-t < 0.8 \text{ GeV}^2$, $-t < 0.9 \text{ GeV}^2$ and $-t < 1.0 \text{ GeV}^2$ are performed and the standard deviations for different E_γ are listed in Table. VII.

In addition, since the energy near threshold is a ambiguous definition, the bins between different input photon energies are relatively small, but there are also some variations of the result among the different data at different photon energies. We calculate the standard deviations from the different photon energies for the extraction of trace anomaly by the experimental data of different collaborations, which is summarised in Table. VIII.

TABLE VII. The standard deviations of trace anomaly contributions (in percentage) with different fitting ranges $|-t| < |-t_{max}|$ at different energies E_γ based on CLAS data [51, 52].

E_γ (GeV)	1.65	1.75	1.85	1.95
Std. Dev.	0.37	0.70	1.13	1.03

TABLE VIII. The standard deviations of trace anomaly contributions (in percentage) with different energies E_γ from different Collaborations (CLAS: $E_\gamma = 1.65, 1.75, 1.85, 1.95$ GeV; SAPHIR: $E_\gamma = 1.70, 1.95$ GeV; LEPS: $E_\gamma = 1.62, 1.72, 1.82$ GeV).

Collaborations	CLAS	SAPHIR	LEPS
Std. Dev.	5.84	2.57	9.22

Through the demonstrations and discussions in this section, we find that the extraction of the proton trace anomaly from experimental data using the model mentioned in this work is dependent on the QCD parameters, especially the quark mass m_q and the strong coupling constant α_s . Based on all the uncertainty analyses discussed above, we give the relative statistical uncertainties of 17.2%, 17.7%, 3.6%, and 8.2%, the total relative systematic uncertainties of 21.4%, 54.2%, 37.2%, and 25.7%, for the trace anomaly determinations from the GlueX, LEPS, CLAS, and SAPHIR data, respectively.

V. CONCLUSIONS AND DISCUSSIONS

In the previous sections we describe in detail about the VMD model [10, 39, 46]. Then we propose how to obtain the trace anomaly in the proton mass decomposition using ϕ and J/ψ near-threshold photo-production experimental data [41, 42, 50, 51]. Based on our extracted results, we give a value of the trace anomaly inside the proton, of which the percentage is from 16% to 24%. Previous Lattice QCD study gives the trace anomaly value about 23% [61]. This work is an attempt to extract the proton trace anomaly using more types of data, and we find that the trace anomaly maybe not depend on the type of the vector meson probe.

The trace anomaly $M_a/M_N = 0.25(1 - b)$ is very sensitive to the parameter r_0 , the ‘‘Bohr’’ radius of vector meson. By Eq. (10) we find that it eventually depends on the constituent quark mass m_q and the running coupling constant α_s . Thus we provide a complete uncertainty analysis in Sec. IV. It also indicates that the trace anomaly we extracted is model parameter dependent, based on the VMD model adopted in this analysis.

The VMD model is successful in describing the vector meson photo-production process, at least as the first step of more extensive theoretical studies. In the VMD model, a real photon fluctuates into a virtual vector meson, which subsequently scatters off the proton target. This model assumption is based on the fact that the vector meson has the same quantum numbers of the photon. The VMD model was used for determining the $\phi - p$, $\omega - p$ and $J/\psi - p$ scattering lengths [62–65]. But the applicability of the VMD model in this case requires special attentions [65]. For a critical review of the VMD model, the papers by Boreskov et. al. [66, 67] and the references therein give a very comprehensive discussions. In this work, the values of quark mass and running coupling are based on the assumptions in the non-perturbative energy region. The strong coupling α_s saturates around 3, which is constrained by the calculation of Lattice QCD [47]. For the “Bohr” radius, more experimental constraints should be found in the future to achieve the goal of reducing the uncertainty. Higher-twist calculations should be investigated as well. From this work, we give the result for the proton anomaly energy, which is similar to the result of the lattice point QCD, and for the first time we provide the statistical and systematical uncertainty analyses. The model uncertainties generated by the current

method in this work are significant and more statistics are needed on the experimental side in future.

Furthermore, the $\Upsilon(1S)$ [68] photo-production data generated by Electron-Ion Colliders in the United States and China [38, 69–72] will become even more important in the future. Since the “Rydberg” energy ϵ_0 of $\Upsilon(1S)$ is higher than that of other quarkonia, Eq. (9) is more valid for the near threshold $\Upsilon(1S)$ production [39, 46]. The theoretical uncertainty from the strong coupling α_s is much smaller at a higher energy scale ϵ_0 . Therefore, the theoretical framework in this work is more suitable for the analysis of near-threshold $\Upsilon(1S)$ photo-production [40] in the future.

ACKNOWLEDGMENTS

We are very grateful to Prof. Fan WANG for his suggestions and the discussions. This work is supported by the Strategic Priority Research Program of Chinese Academy of Sciences under the Grant NO. XDB34030301 and the National Natural Science Foundation of China under the Grant NO. 12005266.

-
- [1] P. W. Higgs, Phys. Rev. Lett. **13**, 508 (1964).
[2] G. S. Guralnik, C. R. Hagen, and T. W. B. Kibble, Phys. Rev. Lett. **13**, 585 (1964).
[3] F. Englert and R. Brout, Phys. Rev. Lett. **13**, 321 (1964).
[4] D. J. Gross and F. Wilczek, Phys. Rev. Lett. **30**, 1343 (1973).
[5] D. J. Gross and F. Wilczek, Phys. Rev. **D8**, 3633 (1973).
[6] D. J. Gross and F. Wilczek, Phys. Rev. **D9**, 980 (1974).
[7] C.-N. Yang and R. L. Mills, Phys. Rev. **96**, 191 (1954).
[8] K. G. Wilson, Phys. Rev. **D10**, 2445 (1974).
[9] M. E. Peskin and D. V. Schroeder, *An Introduction to quantum field theory* (Addison-Wesley, Reading, USA, 1995).
[10] D. Kharzeev, Proc. Int. Sch. Phys. Fermi **130**, 105 (1996), arXiv:nucl-th/9601029.
[11] X.-D. Ji, Phys. Rev. Lett. **74**, 1071 (1995), arXiv:hep-ph/9410274 [hep-ph].
[12] X.-D. Ji, Phys. Rev. **D52**, 271 (1995), arXiv:hep-ph/9502213 [hep-ph].
[13] A. J. Buras, *15th Design Automation Conference Las Vegas, Nevada, June 19-21, 1978*, Rev. Mod. Phys. **52**, 199 (1980).
[14] X. Ji, (2021), arXiv:2102.07830 [hep-ph].
[15] X. Ji and Y. Liu, (2021), arXiv:2101.04483 [hep-ph].
[16] V. Novikov, M. Shifman, A. Vainshtein, and V. Zakharov, Nuclear Physics B **165**, 67 (1980).
[17] V. A. Novikov, M. A. Shifman, A. I. Vainshtein, and V. I. Zakharov, Nucl. Phys. B **191**, 301 (1981).
[18] J. Gasser, H. Leutwyler, and M. E. Sainio, Phys. Lett. **B253**, 252 (1991).
[19] M. Hoferichter, J. Ruiz de Elvira, B. Kubis, and U.-G. Meißner, Phys. Rev. Lett. **115**, 092301 (2015), arXiv:1506.04142 [hep-ph].
[20] X.-L. Ren, X.-Z. Ling, and L.-S. Geng, Phys. Lett. **B783**, 7 (2018), arXiv:1710.07164 [hep-ph].
[21] J. M. Alarcon, J. Martin Camalich, and J. A. Oller, Phys. Rev. D **85**, 051503 (2012), arXiv:1110.3797 [hep-ph].
[22] M. M. Pavan, I. I. Strakovsky, R. L. Workman, and R. A. Arndt, PiN Newslett. **16**, 110 (2002), arXiv:hep-ph/0111066.
[23] G. S. Bali et al. (QCDSF), Phys. Rev. **D85**, 054502 (2012), arXiv:1111.1600 [hep-lat].
[24] Y.-B. Yang, A. Alexandru, T. Draper, J. Liang, and K.-F. Liu (xQCD), Phys. Rev. **D94**, 054503 (2016), arXiv:1511.09089 [hep-lat].
[25] J. M. Alarcon, L. S. Geng, J. Martin Camalich, and J. A. Oller, Phys. Lett. **B730**, 342 (2014), arXiv:1209.2870 [hep-ph].
[26] A. Bottino, F. Donato, N. Fornengo, and S. Scopel, Astropart. Phys. **13**, 215 (2000), arXiv:hep-ph/9909228 [hep-ph].
[27] J. Ellis, K. A. Olive, Y. Santoso, and V. C. Spanos, Phys. Rev. D **71**, 095007 (2005).
[28] J. Ellis, K. A. Olive, and C. Savage, Phys. Rev. D **77**, 065026 (2008).
[29] A. Bottino, F. Donato, N. Fornengo, and S. Scopel, Phys. Rev. D **78**, 083520 (2008).
[30] R. J. Hill and M. P. Solon, Phys. Lett. **B707**, 539 (2012), arXiv:1111.0016 [hep-ph].
[31] J. M. Cline, P. Scott, K. Kainulainen, and C. Weniger, Phys. Rev. D **88**, 055025 (2013).
[32] L. Frankfurt and M. Strikman, Phys. Rev. D **66**, 031502 (2002), arXiv:hep-ph/0205223.

- [33] D. E. Kharzeev, Phys. Rev. D **104**, 054015 (2021), arXiv:2102.00110 [hep-ph].
- [34] R. Boussarie and Y. Hatta, Phys. Rev. **D101**, 114004 (2020), arXiv:2004.12715 [hep-ph].
- [35] Y. Hatta and D.-L. Yang, Phys. Rev. **D98**, 074003 (2018), arXiv:1808.02163 [hep-ph].
- [36] Y. Hatta, A. Rajan, and D.-L. Yang, Phys. Rev. **D100**, 014032 (2019), arXiv:1906.00894 [hep-ph].
- [37] Y.-B. Yang, J. Liang, Y.-J. Bi, Y. Chen, T. Draper, K.-F. Liu, and Z. Liu, Phys. Rev. Lett. **121**, 212001 (2018).
- [38] R. Abdul Khalek *et al.*, (2021), arXiv:2103.05419 [physics.ins-det].
- [39] D. Kharzeev, H. Satz, A. Syamtomov, and G. Zinovjev, Eur. Phys. J. **C9**, 459 (1999), arXiv:hep-ph/9901375 [hep-ph].
- [40] R. Wang, J. Evslin, and X. Chen, Eur. Phys. J. **C 80**, 507 (2020), arXiv:1912.12040 [hep-ph].
- [41] T. Mibe *et al.* (LEPS), Phys. Rev. Lett. **95**, 182001 (2005), arXiv:nucl-ex/0506015.
- [42] A. Ali *et al.* (GlueX), Phys. Rev. Lett. **123**, 072001 (2019), arXiv:1905.10811 [nucl-ex].
- [43] J. Sakurai, Annals of Physics **11**, 1 (1960).
- [44] D. Griffiths, *Introduction to Elementary Particles*, Physics textbook (Wiley, 2008).
- [45] M. E. Peskin, Nucl. Phys. **B156**, 365 (1979).
- [46] D. Kharzeev, H. Satz, A. Syamtomov, and G. Zinovjev, *Quark matter '96. Proceedings, 12th International Conference on Ultrarelativistic Nucleus Nucleus Collisions, Heidelberg, Germany, May 20-24, 1996*, Phys. Lett. **B389**, 595 (1996), arXiv:hep-ph/9605448 [hep-ph].
- [47] Z.-F. Cui, J.-L. Zhang, D. Binosi, F. de Soto, C. Mezrag, J. Papavassiliou, C. D. Roberts, J. Rodríguez-Quintero, J. Segovia, and S. Zafeiropoulos, Chin. Phys. C **44**, 083102 (2020), arXiv:1912.08232 [hep-ph].
- [48] D. Binosi, C. Mezrag, J. Papavassiliou, C. D. Roberts, and J. Rodríguez-Quintero, Phys. Rev. D **96**, 054026 (2017), arXiv:1612.04835 [nucl-th].
- [49] C. Han, G. Xie, R. Wang, and X. Chen, Eur. Phys. J. **C 81**, 302 (2021), arXiv:2010.14284 [hep-ph].
- [50] J. Barth *et al.*, Eur. Phys. J. **A 17**, 269 (2003).
- [51] H. Seraydaryan *et al.* (CLAS), Phys. Rev. C **89**, 055206 (2014), arXiv:1308.1363 [hep-ex].
- [52] B. Dey, C. A. Meyer, M. Bellis, and M. Williams (CLAS), Phys. Rev. C **89**, 055208 (2014), [Addendum: Phys.Rev.C 90, 019901 (2014)], arXiv:1403.2110 [nucl-ex].
- [53] E. Anciant *et al.* (CLAS), Phys. Rev. Lett. **85**, 4682 (2000), arXiv:hep-ex/0006022.
- [54] J. M. Laget, Phys. Lett. B **489**, 313 (2000), arXiv:hep-ph/0003213.
- [55] Q. Zhao, B. Saghai, and J. S. Al-Khalili, Phys. Lett. B **509**, 231 (2001), arXiv:nucl-th/0102025.
- [56] A. I. Titov and T. S. H. Lee, Phys. Rev. C **67**, 065205 (2003), arXiv:nucl-th/0305002.
- [57] A. I. Titov, T. S. H. Lee, and H. Toki, Phys. Rev. C **59**, 2993 (1999), arXiv:nucl-th/9812074.
- [58] A. I. Titov, T. S. H. Lee, H. Toki, and O. Streltsova, Phys. Rev. C **60**, 035205 (1999).
- [59] R. A. Williams, Phys. Rev. C **57**, 223 (1998).
- [60] Y.-s. Oh and H. C. Bhang, Phys. Rev. C **64**, 055207 (2001), arXiv:nucl-th/0104068.
- [61] Y.-B. Yang, J. Liang, Y.-J. Bi, Y. Chen, T. Draper, K.-F. Liu, and Z. Liu, Phys. Rev. Lett. **121**, 212001 (2018), arXiv:1808.08677 [hep-lat].
- [62] I. I. Strakovsky *et al.*, Phys. Rev. C **91**, 045207 (2015), arXiv:1407.3465 [nucl-ex].
- [63] I. Strakovsky, D. Epifanov, and L. Pentchev, Phys. Rev. C **101**, 042201 (2020), arXiv:1911.12686 [hep-ph].
- [64] I. I. Strakovsky, L. Pentchev, and A. Titov, Phys. Rev. C **101**, 045201 (2020), arXiv:2001.08851 [hep-ph].
- [65] L. Pentchev and I. I. Strakovsky, Eur. Phys. J. **A 57**, 56 (2021), arXiv:2009.04502 [hep-ph].
- [66] K. G. Boreskov and B. L. Ioffe, Yad. Fiz. **25**, 806 (1977).
- [67] K. Boreskov, A. Capella, A. Kaidalov, and J. Tran Thanh Van, Phys. Rev. D **47**, 919 (1993).
- [68] I. I. Strakovsky, W. J. Briscoe, L. Pentchev, and A. Schmidt, Phys. Rev. D **104**, 074028 (2021), arXiv:2108.02871 [hep-ph].
- [69] A. Accardi *et al.*, Eur. Phys. J. **A 52**, 268 (2016), arXiv:1212.1701 [nucl-ex].
- [70] X. Chen, PoS **DIS2018**, 170 (2018), arXiv:1809.00448 [nucl-ex].
- [71] X. Chen, F.-K. Guo, C. D. Roberts, and R. Wang, Few Body Syst. **61**, 43 (2020), arXiv:2008.00102 [hep-ph].
- [72] D. P. Anderle *et al.*, (2021), arXiv:2102.09222 [nucl-ex].